

- I- Legends to the *SI Appendix* Figures S1-S9
- II- *SI Appendix*: Figures S1-S9
- III- *SI Appendix*: Table S1
- IV- *SI Appendix*: Materials and methods
- V- *SI Appendix*: References

### I- Legends to *SI Appendix* Figures S1-S9

#### **Fig. S1: The auditory sensory organ and the hair bundle, the sound-receptive structure of sensory hair cells**

(A) The inner ear (upper left panel) contains the vestibule (balance organ), and the cochlea (auditory organ). Running from the base to the apex of the cochlea, the auditory sensory epithelium lies on the basilar membrane. The lower left panel illustrates the frequency-place (tonotopic) map on an F-actin-labeled (red) mouse cochlea. In the auditory sensory epithelium (lower right panel), sensory inner hair cells (IHCs) are organized into a single medial-side row and outer hair cells (OHCs) into three lateral-side rows. A mechanosensitive hair bundle, made of 50 to 300 actin-filled rigid microvilli, known as stereocilia, crowns the apical surface of each hair cell (upper right panel). The tectorial membrane, anchored to the spiral limbus, overlies the sensory epithelium, and is in contact with the tallest stereocilia of OHCs. (B) In the developing hair bundle, a single transient primary cilium, the kinocilium, is located towards the periphery of the hair bundle, attached to adjacent stereocilia of the tallest row by the kinociliary links (KL). The stereocilia are connected by early lateral links (ELL), and ankle links (AL). These transient lateral links are subsequently replaced by the top connectors (TC) in the outer hair cells. The right panel is a magnification of the apical regions of stereocilia from the middle and tall rows of a mature hair bundle. Cadherin-23 and protocadherin-15 form the tip-link, a major component of the mechano-electrical transduction (MET) machinery. These proteins interact with other proteins —proteins including myosin VIIa, harmonin and SANS (Scaffold protein containing Ankryrin and Sterile Alpha Motif (SAM) domains), that are defective in cases of Usher syndrome of type I— at each tip-link insertion point. The MET channels are located at the tips of stereocilia of the short and middle rows.

**Fig. S2: The submembrane scaffold protein Nherf1 and cadherin-23, the protein defective in Usher syndrome type 1D**

(A) Modular structures of cadherin-23 (bait) and Nherf1 ( $\text{Na}^+/\text{H}^+$  exchanger regulatory factor 1), (prey). Nherf1 is also called Ebp50, for Ezrin-radixin-moesin-binding protein of 50 kDa). The position and domain structure of the yeast two-hybrid bait, the cytodomain of murine cadherin-23 containing the fragment encoded by exon 68, and the three independent Nherf1-prey clones isolated are indicated. The common region of three independent prey clones (aa 1-165) is predicted to encode the N-terminal region of Nherf1/Ebp50. Nherf1 contains two PDZ domains, an ERM-binding (EB) domain, and a C-terminal class-1 PDZ-binding motif (asterisk). (PDZ for Post synaptic density protein (PSD95), Drosophila disc large tumor suppressor (Dlg1), and Zonula occludens-1 protein (Zo-1); ERM for Ezrin, Radixin, Moesin). (B) Nherf family members. Nherf1 belongs to a family of four PDZ domain-containing adaptors (Nherf1-Nherf4). Nherf1 and Nherf2 are both composed of two PDZ domains, and an ERM-binding domain that links the proteins to the cytoskeleton. Nherf3 and Nherf4 contain four PDZ domains without any additional regulatory or interaction domains. All Nherf proteins have a C-terminal class-1 PDZ-binding motif (asterisk). (C) Co-immunoprecipitation assays. Co-transfected HEK293 cells producing either the V5-tagged Nherf1 and myc-tagged cadherin-23 cytodomain, or the V5-tagged Nherf1 and the myc-tagged radixin were used for co-immunoprecipitation experiments. The V5-tagged Nherf1 (top) and myc-tagged cadherin-23 cytodomain were co-immunoprecipitated by the anti-V5 antibody. The Nherf1-radixin interaction serves as a positive control. (D-F) Nherf1 and the cadherin-23 cytodomain in the polarized LLC-PK-CL4 epithelial cells. (D) In co-transfected CL4 cells producing Nherf1 and the entire cytoplasmic region of cadherin-23 (Cdh23cyto), the two proteins were co-located in the apical microvilli. (E) In cells producing V5-tagged Nherf1 and a truncated form of cadherin-23 cytodomain that lacks the last nine amino acid residues (Cdh23cyto $\Delta$ 9), the two proteins were not co-located; therefore the interaction probably involves the C-terminal PDZ-binding motif of cadherin-23. (F) CL4 cells were co-transfected with constructs encoding Nherf1 and an hEcadCdh23cyto chimera, composed of the five extracellular cadherin repeats (EC) and transmembrane domain (TM) of the human E-cadherin (hEcadherin) fused to the intracellular domain of the human cadherin-23 (cadherin-23cyto). In these cells, Nherf1 accumulated at the cell-cell junctions together with hEcadCdh23 (arrows), but not elsewhere at the plasma membrane (arrowheads). The schematic diagrams in (D-F) illustrate the domain structure of the fragments produced in CL4 cells.

Scale bars = 10  $\mu\text{m}$ .

### **Fig. S3: Nherf1 spatio-temporal distribution in the auditory sensory epithelium**

(A) The specificity of Nherf1 immunolabeling (green) in the hair bundles. The immunolabeling of the stereocilia observed in wild-type mice is absent from *Nherf1*<sup>-/-</sup> mice (right panel) and is therefore specific for Nherf1. (B) Cochlear sensory epithelia stained for Nherf1 (green) and F-actin (red). At embryonic stages (E15.5, E17, and E18), Nherf1 immunolabeling was detected in the hair bundles of both inner hair cells (IHC) and outer hair cells (OHC). At E15.5, Nherf1 was detected in the actin-rich protrusions that grow on top of the newly differentiated hair cells; similar Nherf1 distributions were also observed at E17.5 and E18.5 in the stereocilia of IHCs, OHCs, and in the microvilli of surrounding supporting cells. On early postnatal days (P0, P3, P5), the protein was no longer detected in IHCs, but the immunoreactivity in the OHC hair bundles increased. Nherf1 immunolabeling was strong at the tips of the stereocilia. This was confirmed by post-embedding immunogold labeling experiments: on E18, the Nherf1-specific gold particles were mainly detected in the apical half of the differentiating stereocilia (upper right panel). The microvilli of surrounding supporting cells were also intense immunolabeled for Nherf1 (arrows in bottom right panel). (C) Isolated OHCs illustrating the strong Nherf1 immunolabeling in the apical regions of the stereocilia (left panels). The immunolabeling of Nherf2, another member of the Nherf family, was stronger in the stereocilia basal region (right panels). Scale bars = 5  $\mu$ m, 250 nm (upper right panel in B).

### **Fig. S4: Abnormal hair bundle shapes and mispositioned kinocilium in the OHC hair bundles of *Nherf1*<sup>-/-</sup> mice**

(A-D) Top views of cochlear whole-mounts from wild-type and *Nherf1*<sup>-/-</sup> mice (scanning electron microscopy). (A) The shape of OHC hair bundles in *Nherf1*<sup>-/-</sup> mice is severely abnormal, as shown from P3 to P8. Instead of the V-shaped hair bundles in wild-type mice (left panels in A), asymmetric OHC hair bundles, with misaligned stereocilia rows, are observed in *Nherf1*<sup>-/-</sup> mice. (B) Left panel: the numbers of stereocilia per OHC hair bundle were not significantly different between *Nherf1*<sup>-/-</sup> and wild-type animals ( $p > 0.05$ ). Right panels: the lateral links that connect adjacent stereocilia in their apical (upper) and basal (lower) parts at P3 are preserved in *Nherf1*<sup>-/-</sup> hair bundles. (C) Mispositioned kinocilium in the OHC hair bundles in the cochlear basal region of *Nherf1*<sup>-/-</sup> mice. Upper panels: The upper schematic representation illustrates hair bundle orientation and the method used to measure the angular deviation of the kinocilium with respect to the planar cell polarity (PCP) axis. TRITC-phalloidin was used to label the stereocilia (red), and an anti-acetylated tubulin

antibody to label the kinocilia (green). In the scanning electron micrographs (right panels), kinocilia were artificially labeled in green to facilitate visualization. Lower panels: The mean absolute deviations ( $\pm$  sem) of the kinocilia in the three rows of OHCs were between  $12\pm 1^\circ$  and  $18\pm 1^\circ$  in *Nherf1*<sup>-/-</sup> mice, and between  $5\pm 1^\circ$  and  $9\pm 2^\circ$  in wild-type mice. In wild-type mice, 58% of the kinocilia were within  $7^\circ$  of the PCP axis; in *Nherf1*<sup>-/-</sup> mice, only 26% of the kinocilia were within  $15^\circ$  of the PCP axis. Scale bars = 1  $\mu$ m (A, B), 5  $\mu$ m (C). \*\* and \*\*\* denote  $p < 0.01$  and  $p < 0.001$ , respectively (Student's *t* test).

**Fig. S5: Abnormal OHC hair bundle shapes and TM imprints predominate in the cochlear basal region in *Nherf1*<sup>-/-</sup> mice**

(A-C) Various abnormal shapes of the OHC hair bundles are observed in *Nherf1*<sup>-/-</sup> mice: they include wavy (red), linear (yellow) and hooked (green) hair bundles. (B) Examples of wild-type and *Nherf1*<sup>-/-</sup> hair bundles, illustrating the anomalies of OHC, but not IHC hair bundle shapes in *Nherf1*<sup>-/-</sup> mice. (C) At the cochlear apex of *Nherf1*<sup>-/-</sup> mice, the shapes of few OHC hair bundles were affected and only mildly, whereas most of the OHC hair bundles at the cochlear base were mis-shaped. (D, E) Imprints of the tallest OHC stereocilia in the tectorial membrane (TM). (D) Upper panels: In *Nherf1*<sup>-/-</sup> mice, almost all of the OHC imprints ( $90\pm 5\%$ , see lower left panels) in the lower face of the TM in the cochlear basal region were mis-shaped (green in the histograms), whereas only  $15\pm 3\%$  were abnormal in the cochlear apical region, and in these cases the anomalies were minor (lower right panels). (E) Labeling of the stereocilia imprints of the three OHC rows of in the TM using an anti-stereocilin antibody (green) shows the abnormal imprints in *Nherf1*<sup>-/-</sup> mice.

Scale bars = 5  $\mu$ m (A, C), 1  $\mu$ m (B, D, E).

**Fig. S6: Distortion product otoacoustic emissions (DPOAEs) and auditory brainstem responses (ABR) recordings in *Nherf1*<sup>-/-</sup> mice**

(A) Distortion product otoacoustic emissions (DPOAEs) in P20-P28 wild-type (black) and *Nherf1*<sup>-/-</sup> (red) mice. Tests were carried out before P30 to avoid any interference from age-related high frequency hearing loss. DPOAEs for 10 kHz and 20 kHz tone stimuli are shown. DPOAE amplitudes in *Nherf1*<sup>-/-</sup> mice, within the normal range at 10 kHz, were significantly lower than normal at 20 kHz. (ns) and \*\*\* denote no statistically significant difference, and a

significant difference with  $p < 0.0001$ , respectively (2-way ANOVA). (B) Examples of ABR recordings at 10 kHz (75 dB SPL) in a wild-type mouse, and at 32 kHz in wild-type (at 75 dB SPL) and *Nherf1*<sup>-/-</sup> (at 75 and 95 dB SPL) mice. The latency of the 32 kHz ABR-wave I (arrows) in the *Nherf1*<sup>-/-</sup> mouse jumped from 1.60 to 1.25 ms when the stimulus level increased from 75 dB SPL (light red trace) to 95 dB SPL (dark red trace), but nevertheless remained 0.20 ms longer than the wave-I latency at 32 kHz, 75 dB SPL in a wild-type ear and was more similar to the wave-I latency at 10 kHz in this control ear (blue trace).

**Fig. S7: Masking tuning curves (TCs) in wild-type, *Nherf1*<sup>-/-</sup>, and *Nherf2*<sup>-/-</sup> mice**

(A) Examples of masking tuning curves (TCs) for 20 kHz (left panels), and 32 kHz and 40 kHz (middle panels) probe tones in P20-P25 wild-type and *Nherf1*<sup>-/-</sup> mice. The TCs represent, against masker frequency, the smallest intensity of the masker able to decrease by half the compound action potential elicited in the auditory nerve by a probe tone-burst at 5-10 dB above the ABR threshold. In the wild-type mouse (upper panels), the TCs display a characteristic narrow V-shaped dip corresponding to the most efficient masker tone at or near the probe frequency (20, 32 or 40 kHz), and near the probe intensity. The shallow slope of TC curves toward lower frequencies defines a broad low-frequency tail, in which masker tones have to be 30-50 dB above the probe intensity to exert masking. By contrast, in the *Nherf1*<sup>-/-</sup> mouse (lower panels), hardly any masking was present for masker frequencies around the probe tone at 20 kHz, 32 kHz or 40 kHz. Only in some but not all *Nherf1*<sup>-/-</sup> mice, a dip-like minimum around the probe frequency (32 kHz) was observed for a 32 kHz masker, but with intensities exceeding 100 dB SPL (bottom right panel). In all these mutant mice, the most efficient masker (dip of the V-shaped curve) was in the lower frequency interval, between 7 kHz and 14 kHz. The most efficient masker for both 32 kHz and 40 kHz probe tones in a given ear was at the same frequency, 12.5 kHz in the example shown in the bottom middle panel. Furthermore, the two TCs coincided within 5 dB over the whole masker-frequency range. (B) Growth of masker curves experiments. Average ratios ( $\pm$ sd) of growths of masker and probe tones (in dB per dB) in wild-type and *Nherf1*<sup>-/-</sup> mice, when probe and masker frequencies were similar (on-frequency) or very different (off-frequency). The on-frequency configuration cannot be tested in *Nherf1*<sup>-/-</sup> mice because masking starts appearing only at masker intensities  $> 100$  dB SPL. Individual growth-of-masker plots are depicted in Fig. 4A.

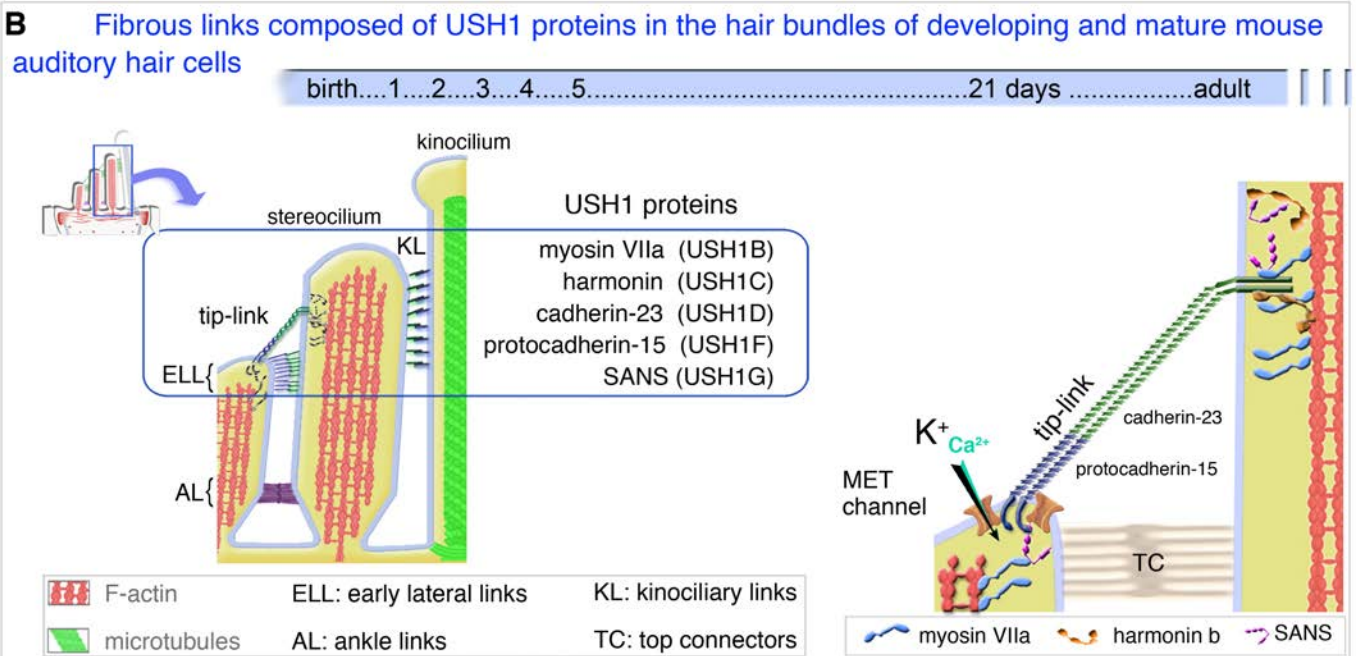
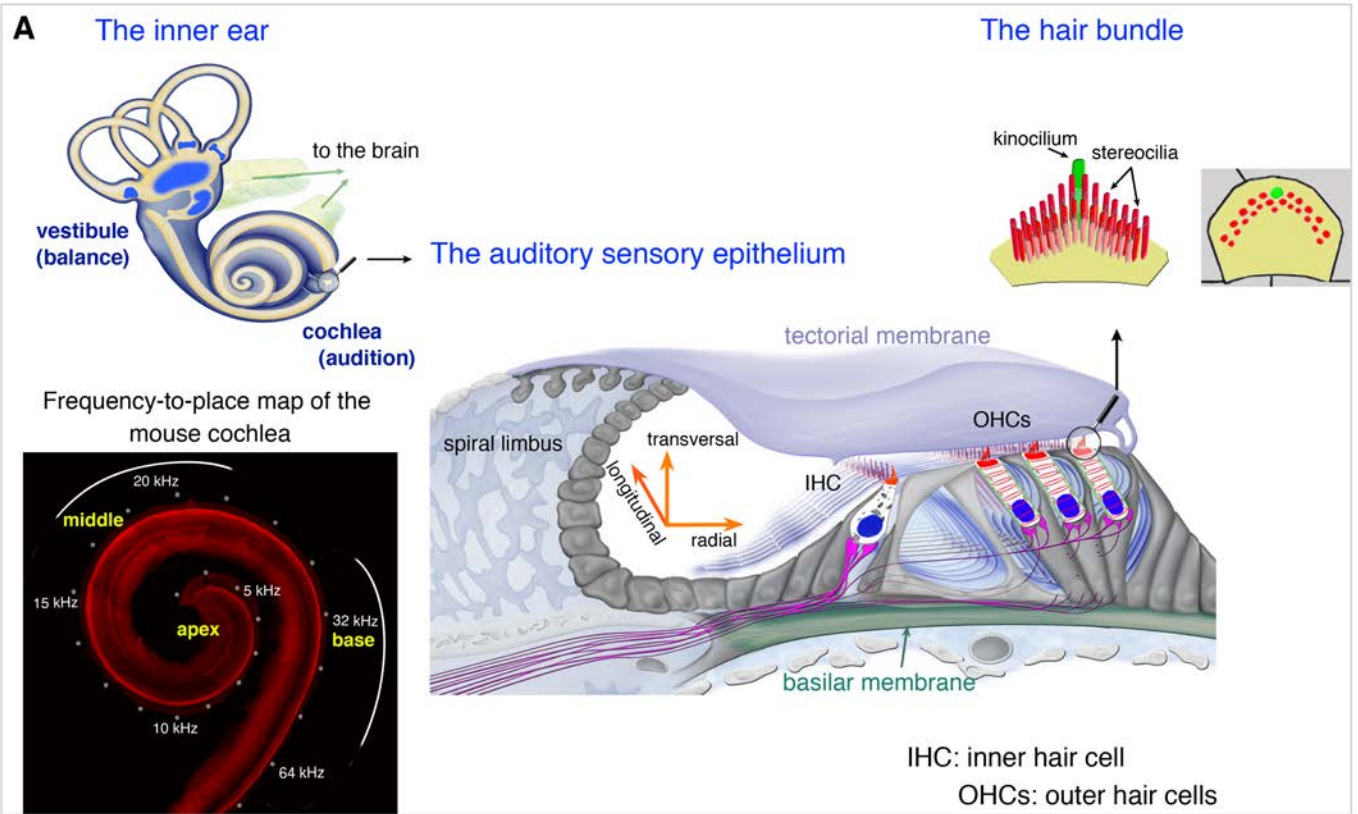
**Fig. S8: The acoustic source of a 32 kHz tone-burst stimulus, and the auditory characteristics and masking tuning curves in wild-type, *Nherf1*<sup>-/-</sup>, and *Nherf2*<sup>-/-</sup> mice**

(A, B) **Tone-burst stimuli at high frequencies and related spectral splatter.** We tested the acoustic source of the high-frequency probe stimuli for the presence of low-frequency spectral splatter: by eliciting ABR responses in the normally sensitive low-frequency cochlear region of *Nherf1*<sup>-/-</sup> mice, this could account for the observed shift of masking toward low frequencies. (A) Time course of acoustic pressure recorded by a microphone in the ear canal of a mouse, in response to a 32-kHz tone burst (brown line). In its low-pass filtered version (green, vertical axis expanded x30), most of the spectral components above 15 kHz have been strongly attenuated and a small low-frequency artifact is revealed, made up of about one period of an oscillation around 10 kHz at onset, and one at offset, in close temporal correspondence with the stimulus at the tone-burst frequency. (B) The frequency spectrum of a 32 kHz tone-burst measured *in situ* by a calibration microphone is represented in orange. The level of the main peak at 32 kHz serves as a reference (0 dB) for the vertical dB scale. The average difference between ABR thresholds at the measured frequency at 32 kHz in *Nherf1*<sup>-/-</sup> mice is presented in red, and that in the *Nherf1*<sup>-/-</sup> most extreme ear among those tested is in blue. Analysis of the frequency spectrum revealed a low-frequency onset artifact in the 6-14 kHz frequency interval (asterisk above orange line), 45 dB below the level of the main 32 kHz tone-burst regardless of intensity of the sound, too small to elicit spurious ABR responses (similar data were collected at 20 kHz). Thus, the spectral splatter cannot contribute to the measured 32 kHz-ABR thresholds even at 10 kHz, at which spectral splatter remains 12 dB too weak on average (and 2-dB too weak, in the less favorable ear) to produce any ABR. When the level of the 32-kHz tone-burst is well in excess of 65 dB SPL, small ABR contributions can be generated in cochlear regions tuned to low frequencies, but these sound levels are high enough that IHCs in the basal cochlea can be stimulated directly by the main tone burst in a broad region around its CF place, despite the absence of OHC activity. These basal contributions to ABRs grow fast and likely overwhelm any contribution from the apex. (C) Difference in dB between thresholds at frequencies > 15 kHz and threshold at 15 kHz, for ABR (plain lines) and DPOAEs (dashed lines), in *Nherf1*<sup>-/-</sup> (red lines) and *Nherf2*<sup>-/-</sup> (green lines) mice. The DPOAE thresholds were more severely affected in *Nherf1*<sup>-/-</sup> (dashed red line) than in *Nherf2*<sup>-/-</sup> mice (dashed green line). However, the changes in ABR thresholds at increasing tone-burst frequencies were similar in the two mouse mutants, such that they are similarly sensitive to the biasing effect on ABR thresholds of a hypothetical low-frequency spectral splatter affecting the spectra of high-frequency tone-bursts (20 kHz and above). (D) The same acoustic setup was used to establish the masking tuning curves (TCs) in *Nherf1*<sup>-/-</sup> and *Nherf2*<sup>-/-</sup> mice. Unlike the masking TC for

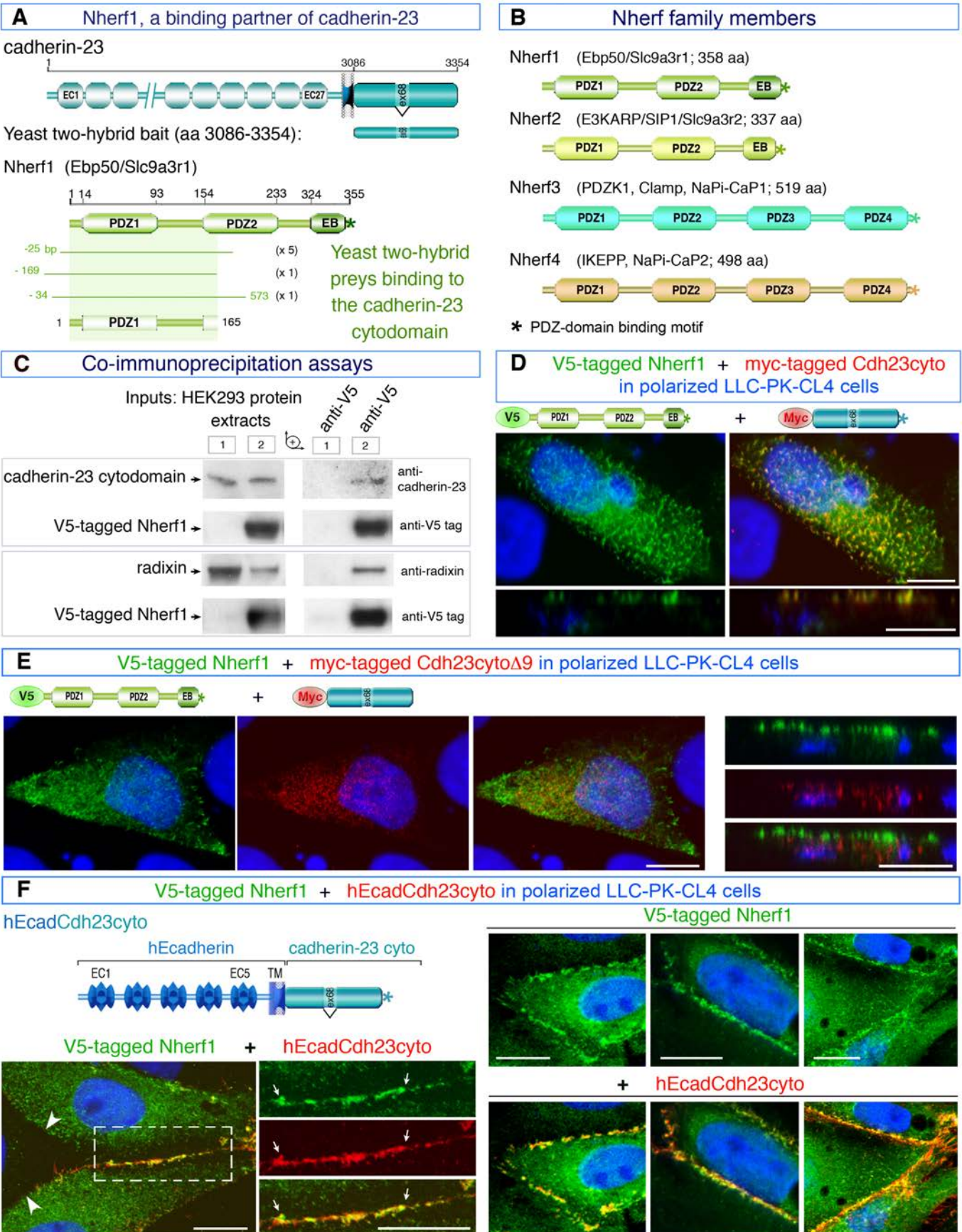
*Nherf1*<sup>-/-</sup> mice (lower left panel, same as S7A), the masking TC for *Nherf2*<sup>-/-</sup> mice (lower right panel) was centered near the probe frequency, and all changes in their characteristics followed the conventional pattern: for a 32 kHz probe, the TC dip was enlarged and elevated but remains near the probe frequency and the low-frequency tail was sensitive as in controls. The masker threshold intensities in the tail region were about 15 dB higher than those in the dip frequency interval. These observations are consistent with acoustic calibration, and rule out any possibility of participation of low-frequency transient artifacts of the acoustic stimulus in the functional pattern and masking TCs of *Nherf1*<sup>-/-</sup> mice.

**Fig. S9: Spatio-temporal distribution of Nherf2 in cochlear hair cells, and OHC hair bundle architecture in *Nherf2*<sup>-/-</sup> mice**

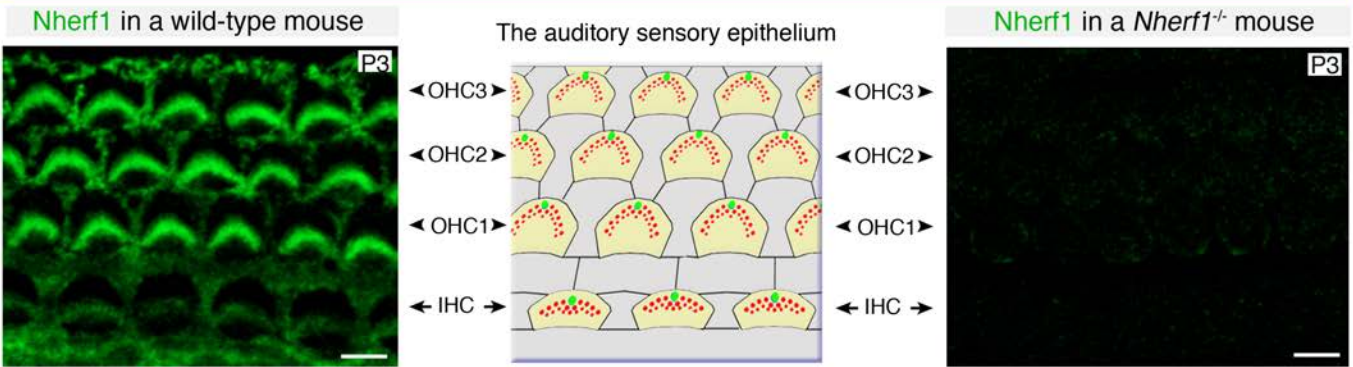
(A) The distribution of Nherf2 in the auditory sensory organ was analyzed at embryonic and postnatal stages. Nherf2 immunostaining (green) was detected as early as embryonic day E15.5 in the emerging stereocilia of both IHCs and OHCs. The staining was more intense at post-natal stages (P0, P5, and P15, and P90), especially in the stereocilia of IHCs. Most Nherf2 staining was located in the stereocilia basal region, as shown in an IHC hair bundle at P90 (right panels). (B) The specificity of the Nherf2 immunolabeling (green) in the hair bundles (F-actin labeling, red) of the wild-type mice was confirmed by its absence from *Nherf2*<sup>-/-</sup> mice. (C) Scanning EM analysis of the OHC hair bundles in *Nherf2*<sup>-/-</sup> mice. At early post-natal stages (P5-P7), the OHC hair bundle shapes in *Nherf2*<sup>-/-</sup> mice were approximately normal, and similar to those in wild-type mice. However, some abnormally shaped OHC hair bundles were present at post-hearing stages, as illustrated here on P21 (arrows). Despite missing or fused stereocilia in the short and middle rows of some hair bundles in P21 *Nherf2*<sup>-/-</sup> mice, the OHC imprints on the lower surface of the TM are roughly normal all along the cochlea (see upper right panel). Scale bars = 1  $\mu$ m.



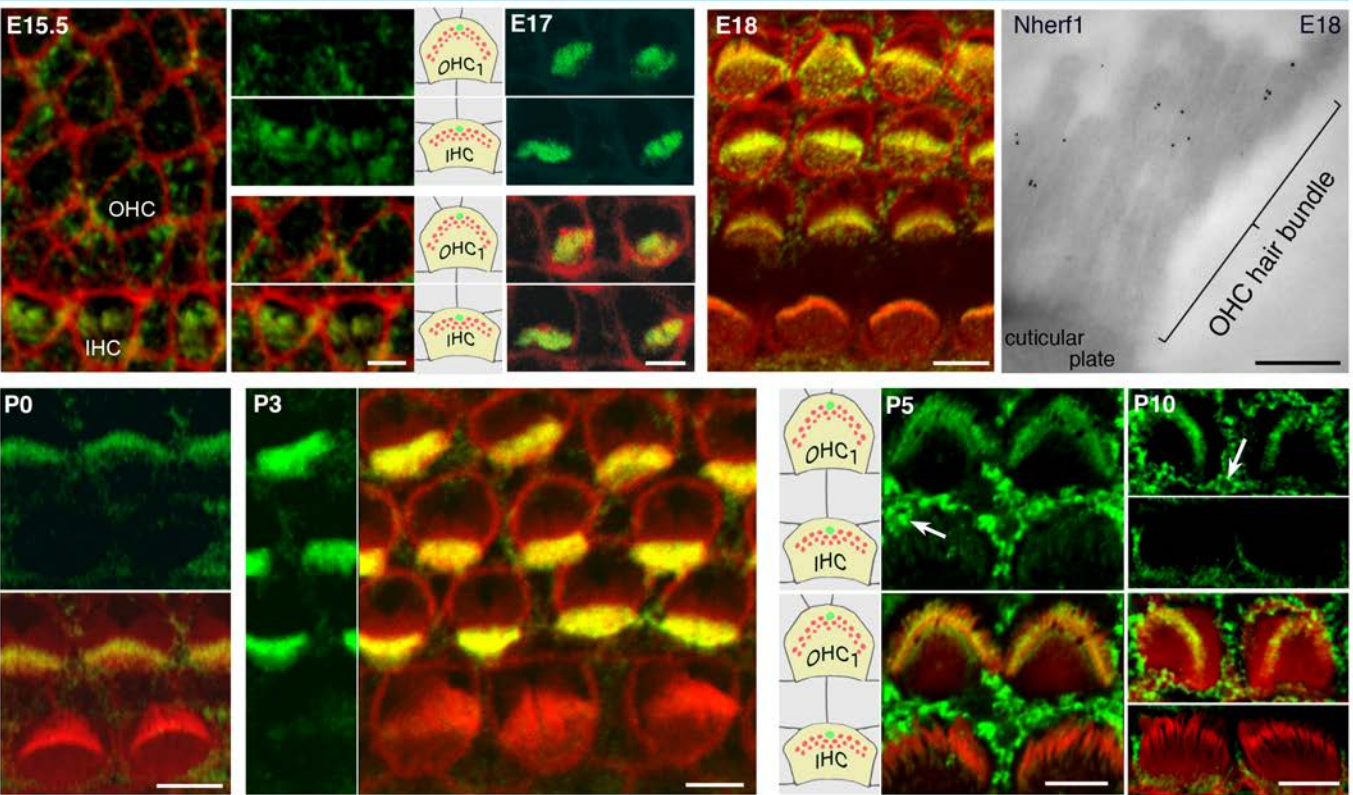




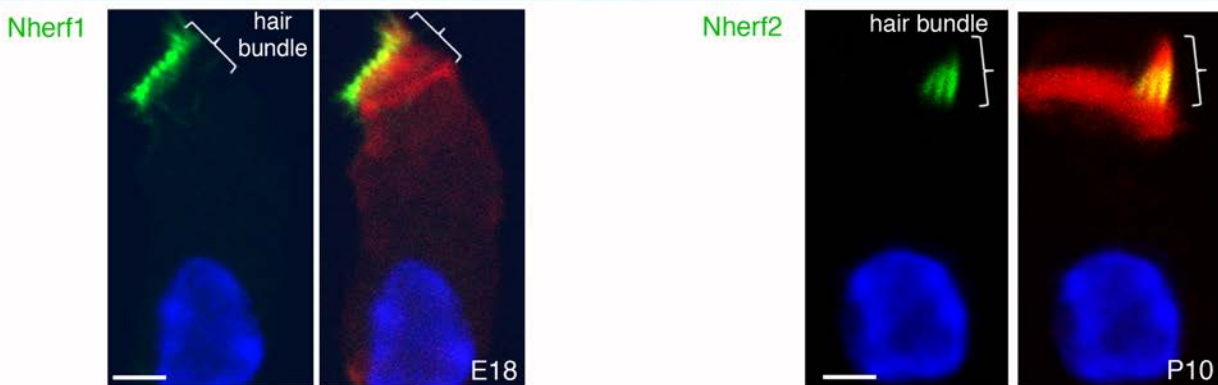
**A** Validation of the anti-Nherf1 antibody in a *Nherf1*<sup>-/-</sup> mouse

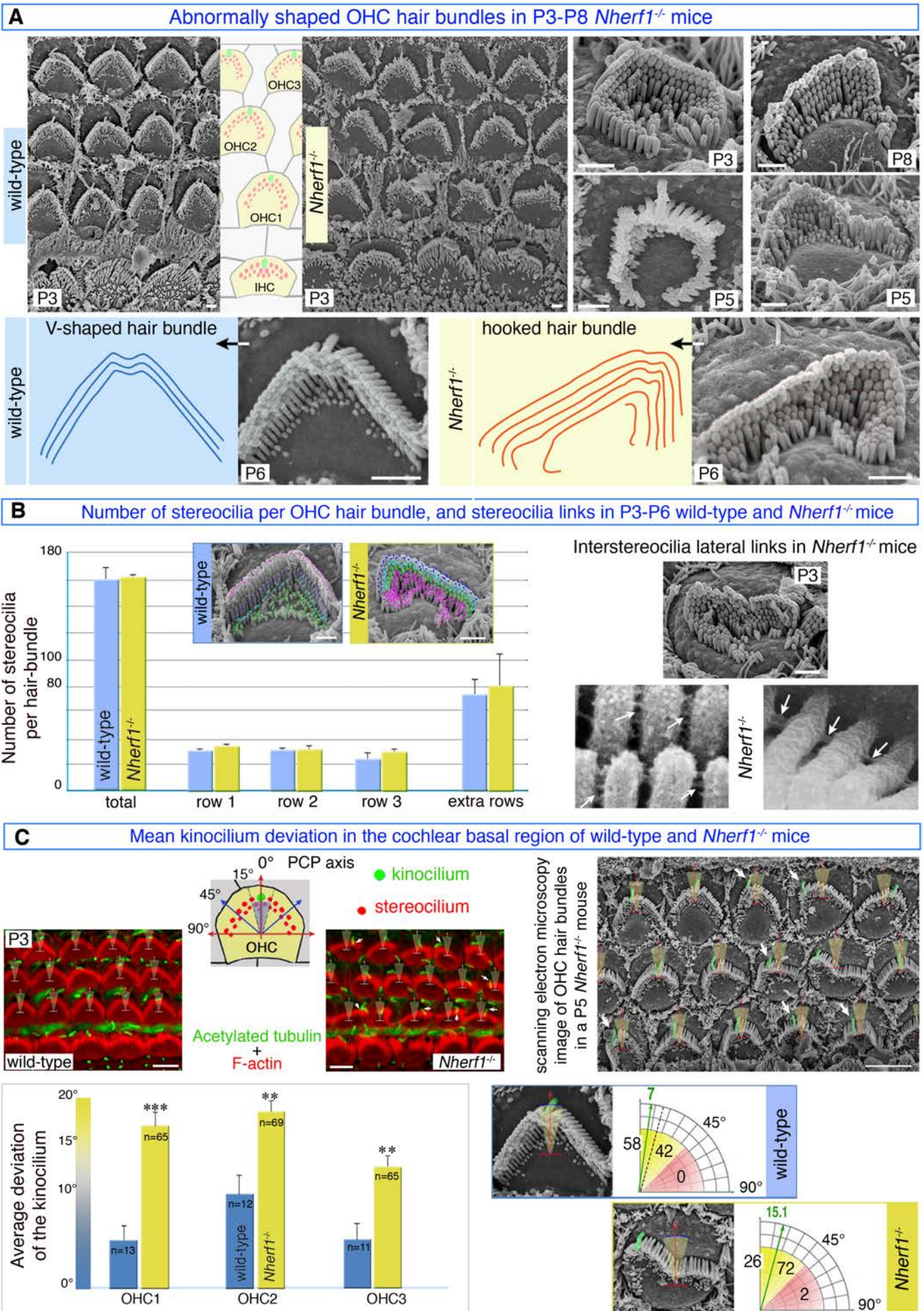


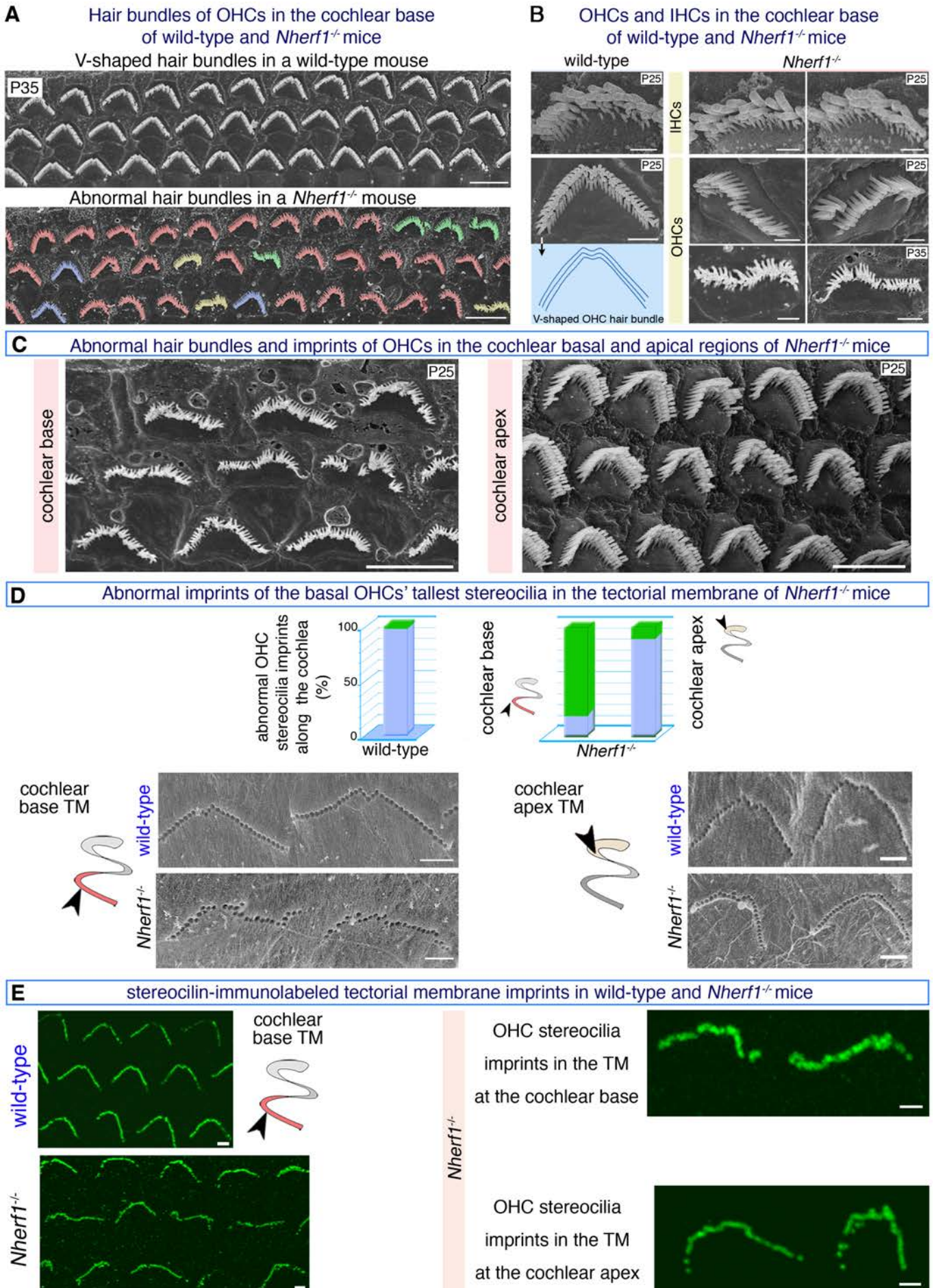
**B** Nherf1 + F-actin at embryonic and post-natal stages



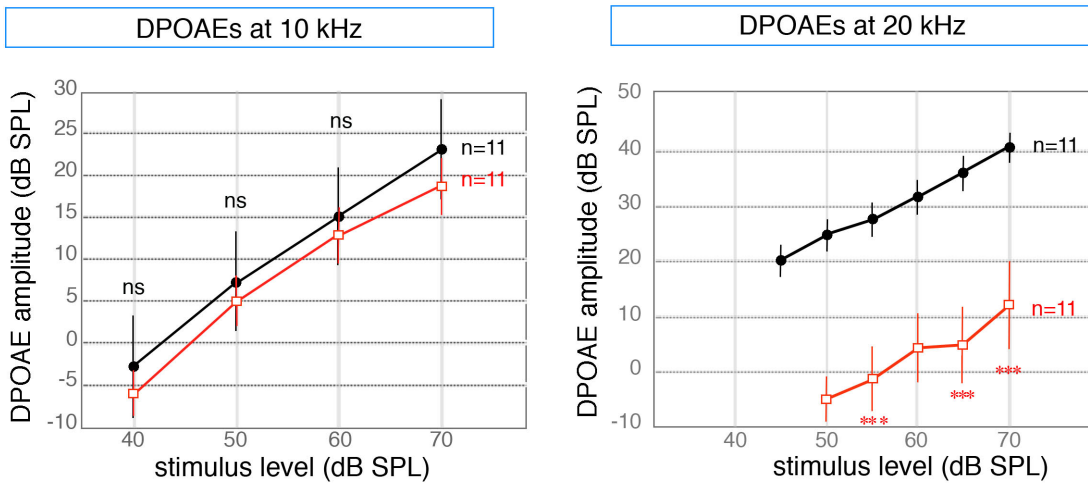
**C** Nherf1, Nherf2 and F-actin in isolated outer hair cells



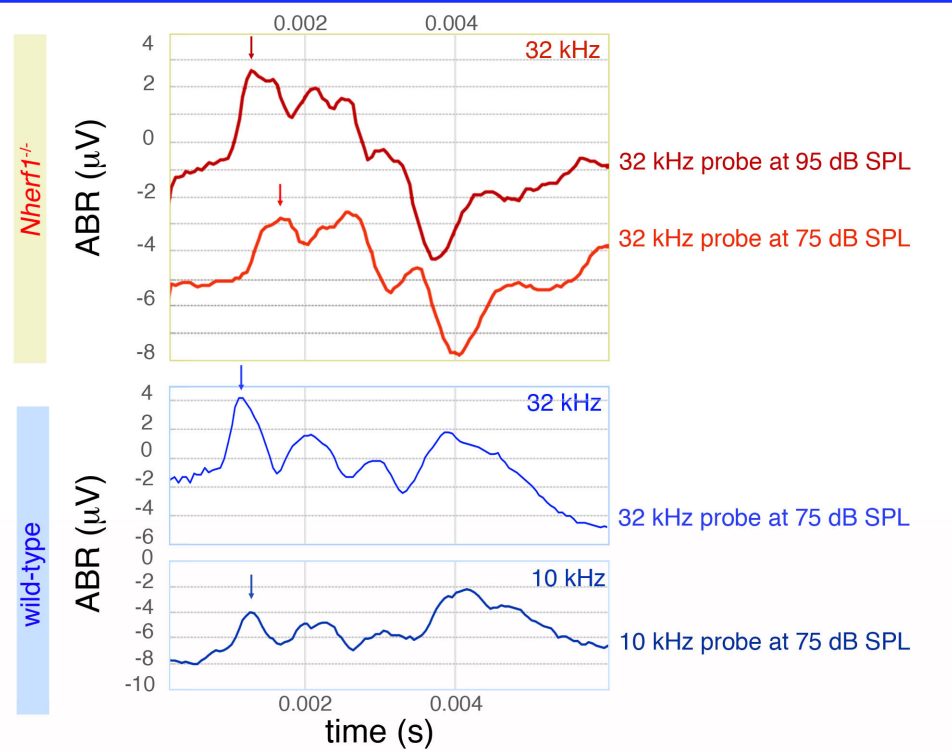




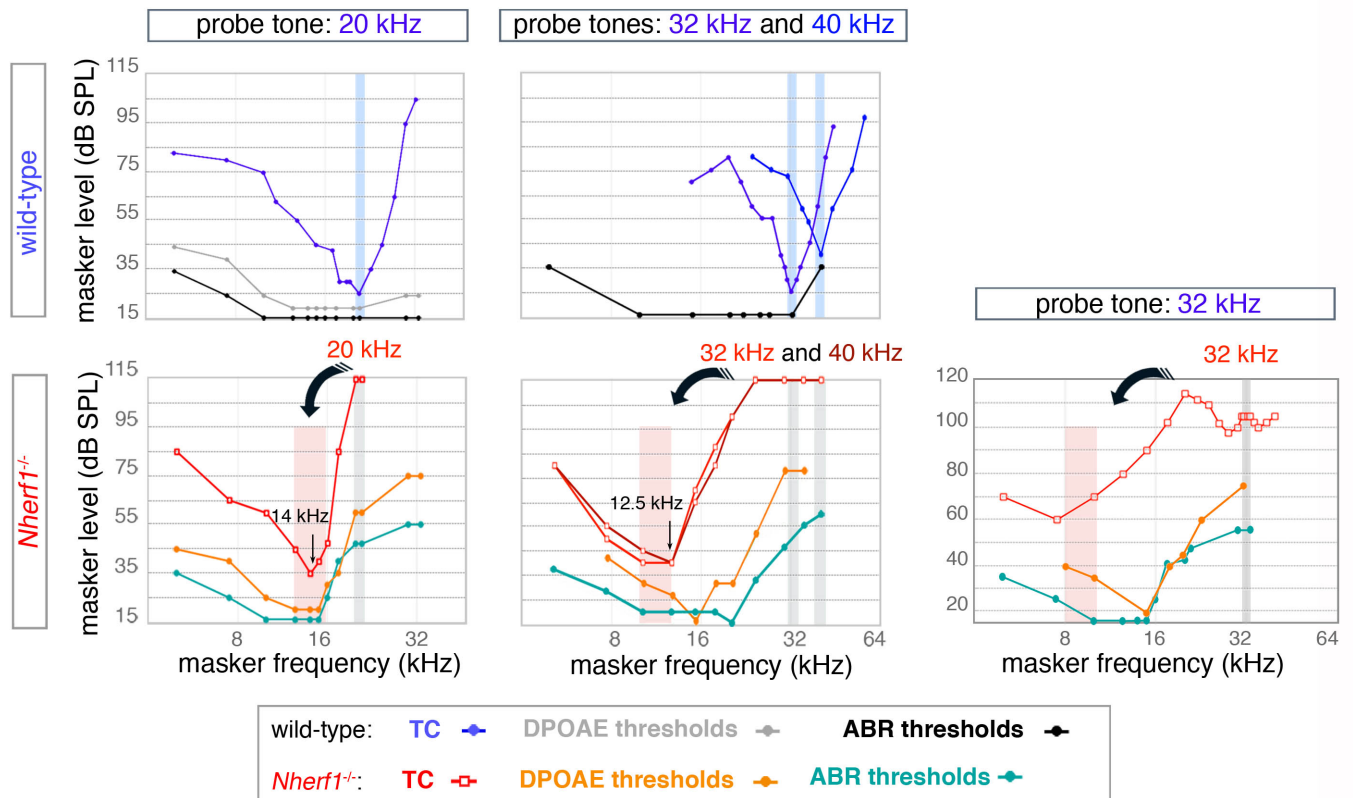
**A** Distortion product otoacoustic emissions (DPOAEs) at 10, and 20 kHz in wild-type (●), and *Nherf1*<sup>-/-</sup> (□) mice



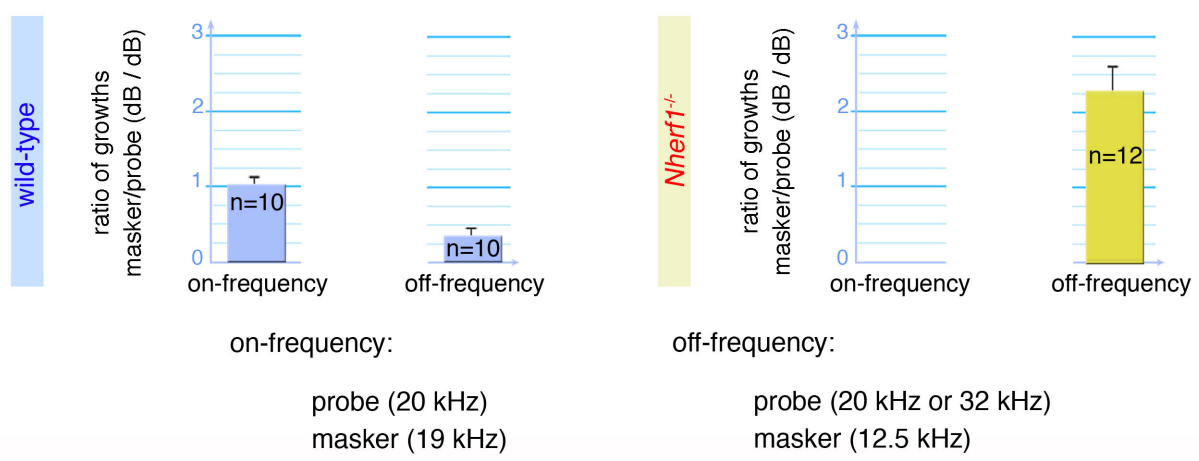
**B** ABR wave I latencies in wild-type and *Nherf1*<sup>-/-</sup> mice

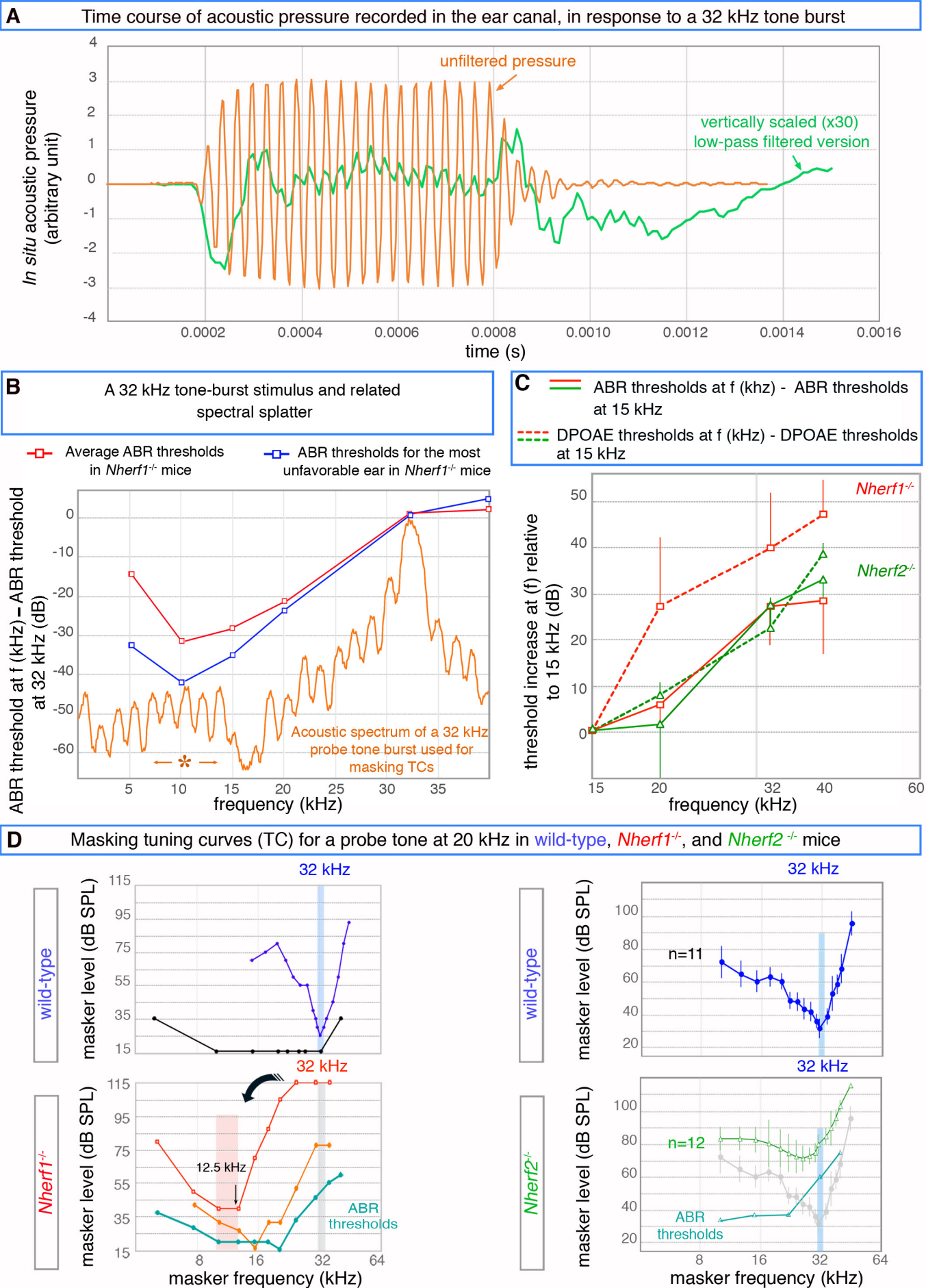


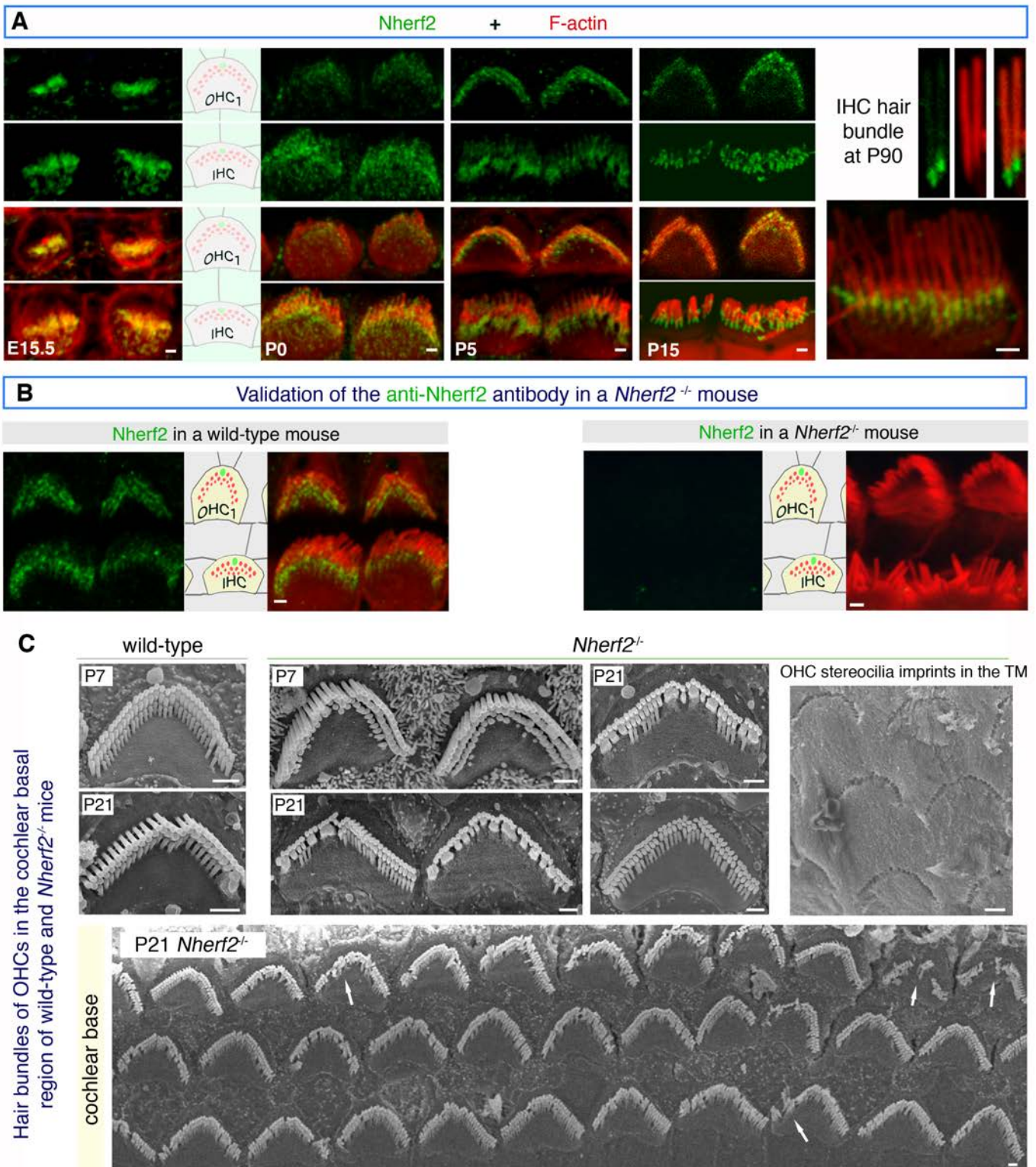
**A** Masking tuning curves (TC) in *wild-type* and *Nherf1<sup>-/-</sup>* mice



**B** Growth of masking for on- and off-frequency conditions in *wild-type* and *Nherf1<sup>-/-</sup>* mice









### III- SI Appendix: Table S1:

**Table S1:** *Nherf1*<sup>-/-</sup> mice, off-frequency situation, probe at 32 kHz; maximally efficient masker at ~12.5 kHz

Interpretative framework	True probe frequency	CF at place of interference	Compression of probe	Compression of masker	Expected GOM
Spectral splatter	12.5 kHz	12.5 kHz	+	+	1 dB per dB
Tail hypersensitivity	32 kHz	32 kHz	+	0	0.3 dB per dB
Off-frequency detection	32 kHz	~12.5 kHz	0	+	~ 3 dB per dB

Note: If the presumed off-frequency detection occurs over a broad cochlear region, for example because the mechanism of apical propagation at its origin has little frequency specificity, efficient maskers may act despite not corresponding exactly to the CF, as CFs in the region of interference span a broad range. Consequently, maskers would not be compressed at the maximum rate and the GOM would be less than the inverse of the maximum compression rate, thus, < 3 dB per dB. On the basis of this reasoning, the only interpretative framework that can explain the GOM data is off-frequency detection, unless tail hypersensitivity in *Nherf1*<sup>-/-</sup> mice is due to a novel type of OHC dysfunction such that places with normally high CFs both respond much better to low frequencies than to the CF and actively process low-frequency sounds in such a way that compression happens at low frequencies while no longer happening at the CF. However, the currently available evidence overwhelmingly suggests that compression requires functionally operating OHCs and is restricted to frequencies near the CF (1).

#### **IV- SI Appendix: Materials and methods:**

##### **Subtractive inner ear cDNA library and yeast two-hybrid screening**

To isolate genes preferentially expressed in hair cells, cDNAs from the sensory epithelia of P0-P4 mouse vestibular end organs were subtracted with cDNAs from the non-sensory cartilaginous and membranous parts of the P0-P4 semi-circular canals, and with P2 liver and P15 dorsal root ganglion cDNAs; a modified RDA (representational difference analysis) technique was used as described elsewhere (2).

For the yeast-two hybrid screening, the intracellular region of cadherin-23 (NM-022124; amino acid residues 3086-354) that includes the 35 amino acid residues encoded by exon 68 was used as a bait to screen a cDNA library derived from microdissected vestibular sensory epithelia of P2 to P6 mice (3).

##### **DNA constructs**

A cDNA encoding the full-length *Nherf1* (NM\_012030) was obtained from the mouse inner ear cDNAs, and inserted into the pcDNA3.1 vector. The cDNAs encoding fragments of cadherin-23 were transferred into appropriate vectors as follows. The cDNA encoding the intracellular region of the cadherin-23 isoform that contains the exon 68-encoded fragment (CDH23+ex68, NM-022124; amino acid residues 3086-3354) was inserted into pCMV-tag3B; and the recombinant cDNA encoding a chimera composed of the extracellular and transmembrane domains of human E-cadherin fused to the cytoplasmic domain of human cadherin-23 lacking the alternative exon 68-encoded fragment (NP\_001165405, amino acid residues 847-079) was ligated into pCDNA3.1 (3). A QuikChange XL site-directed mutagenesis kit (Stratagene) was used to delete the segment encoding the last nine amino acid residues of CDH23+ex68 (pCMV-tag3B).

##### **Immunofluorescence and electron microscopy analyses**

The distribution of *Nherf1* was studied in RJ Swiss mice (Janvier Labs, France). Embryonic day 0 (E0) was determined by vaginal plug detection, and the day of birth was defined as P0. *Nherf1*<sup>-/-</sup> mice (C57BL/6J background) (4), *Nherf2*<sup>-/-</sup> mice (5), and *Cdh23*<sup>v2j/v2j</sup> mice (6) were used. Experiments with animals were carried out using protocols approved by the Animal Use Committee of INSERM and Institut Pasteur.

LLC-PK1-CL4 cells derived from pig kidney (gift from J.R. Bartles, Northwestern University Feinberg School of Medicine, USA) were used as previously described (7). Samples (whole mount preparations of the organ of Corti, cryosections, isolated hair cells, or LLC-PK cells on glass coverslips) were processed for immunofluorescence as previously described (8). Briefly, after blocking in 20% goat serum in phosphate-buffered saline (PBS), and overnight incubation with the primary antibody, sections were rinsed in PBS, incubated with appropriate secondary antibodies for 1 hour at room temperature, and counterstained with DAPI. Images were collected using a Zeiss LSM510 Meta confocal microscope.

For scanning electron microscopy, inner ears were fixed in 2.5% glutaraldehyde in 0.1 M phosphate buffer (pH 7.3) for 2 hours at room temperature. The samples were washed several times with the buffer alone, and cochlear sensory epithelia were finely dissected and processed using the osmium tetroxide/thiocarbohydrazide (OTOTO) method, as previously described (9).

For immunoelectron microscopy, fixed specimens were incubated in pure LR White overnight at room temperature, processed as described (6), and studied under a transmission electron microscope (H-7100, HITACHI, Japan).

The anti-Nherf1 polyclonal antibody (Abcam) was raised against an internal peptide (amino acid residues 286-302) located between the PDZ2 and EB domains of the human protein. Its specificity was verified by immunofluorescence experiments using *Nherf1*<sup>-/-</sup> mice as negative controls (Supplementary Fig. S2).

The following primary antibodies were used: affinity-purified rabbit polyclonal antibodies against cadherin-23 (3), anti-stereocilin (10), anti-Nherf2 (HPA001672, Sigma), mouse anti-acetylated tubulin (Sigma), and mouse anti-V5-tag (Invitrogen). TRITC-phalloidin (Sigma) and DAPI (1 µg/ml; Sigma) were used to label F-actin and cell nuclei, respectively.

### **Kinocilium deviation analysis**

The deviation of the kinocilium in the outer hair cells at the cochlear base was determined by measuring the angle formed by two crossing lines as described previously (6). The first line was drawn mediolaterally along the symmetry/PCP axis of the cell, thereby running through the expected position of the kinocilium. The second line was drawn between the center of the hair cell surface and the observed position of the kinocilium. Data were

analyzed with the Excel software (Microsoft Office), and Student's *t*-test was used to determine the statistical significance of differences.

### ***In vivo* auditory tests**

To test hearing, distortion product otoacoustic emissions (DPOAEs), auditory brainstem responses (ABRs), cochlear microphonic (CM) electrical potential, and compound action potentials (CAPs) were recorded in anesthetized mice, and analyzed as described elsewhere (10, 11). Animals were anesthetized with a mixture of ketamine (150 mg/kg) and levomepromazine (2 mg/kg), with additional half doses given every 30 min. Their temperature was kept at 37 °C with a regulated heating blanket.

For DPOAE measurements,  $f_1$  and  $f_2$  stimuli were carefully applied through different earphones and tubing to avoid nonlinear interactions on earphone membranes. Only the cubic difference tone at  $2f_1-f_2$ , the most prominent one from the ear (12), was detected. This DPOAE comes mainly from the place where there is maximum overlap between basilar membrane vibrations to  $f_1$  and  $f_2$ , i.e., near the place tuned to  $f_2$ . Therefore, the  $2f_1-f_2$  DPOAE was plotted against  $f_2$ . The  $f_2$  frequency was swept from 5 to 32 kHz in  $1/8^{\text{th}}$  octave steps, with  $f_1$  chosen such that the frequency ratio  $f_2/f_1$  was 1.20. The intensities of the two tonal stimuli at  $f_1$  and  $f_2$  were the same, from 20 to 80 dB SPL in 5 dB steps. We used an IHS system (IHS, Miami, FL, USA) driven by SmartOAE software (IHS) in the growth-function mode, between 5 and 32 kHz. Measurements were extended above 32 kHz, to  $f_2 = 40$  kHz, using a pair of waveform generators (Wavetek 70), and the resulting sound in the ear canal was collected by the IHS microphone, while the  $2f_1-f_2$  DPOAE amplitude was measured by an FFT analyzer (OnoSokki). The DPOAE threshold was defined as the weakest stimulus eliciting a DPOAE significantly above the background noise level, estimated from the spectral lines closest to  $2f_1-f_2$  in the 0.5 s sound samples collected in the ear canal.

For CAP measurements, a Teflon-coated silver-wire electrode was surgically inserted into the round-window niche, with the negative and ground electrodes subcutaneously placed on the skull and neck regions. The electrocochleogram was collected by a Grass preamplifier (gain x10,000) and numerically averaged (CED 1401+ processor) in synchrony with the stimulus (x32). For ABR recordings, three steel electrodes were inserted (negative and ground as for CAP measurements, and the positive in the mastoid region). The electroencephalogram was collected by the preamplifier with a x100,000 gain, and numerically averaged over 256 epochs.

The acoustic system that generated the tone-bursts for ABR and CAP measurements was controlled for the spectrum and level of onset and offset transient artifacts. These artifacts arise whenever a short, high-frequency voltage burst at frequency  $f$  drives an earphone. In ears with a large difference in sensitivity between high- and low-frequency regions, the low-frequency spectral splatter induced by these transients must not be large enough to trigger synchronous neuronal responses from the cochlear region tuned to low frequencies. If, at the same time, the energy of the main spectral peak at  $f$  does not exceed the threshold of the cochlear place tuned to it, the ABR and CAP would represent responses to the low-frequency artifact, and thus not be representative of the cochlear sensitivity to  $f$ . Likewise, masking TCs would display a dip at low frequencies, because low-frequency maskers would be most efficient at masking an artifactual CAP.

For both ABRs and CAP, the sound stimuli used were tone-bursts produced by a Wavetek-70 arbitrary waveform generator (2-period rise and decay times, 16-period plateau) and sent to a Radioshack tweeter (40-1376, 8 Ohm – 70 W) connected to a conical tip. Tone-burst frequencies were in the range 5 to 40 kHz. At every frequency, the threshold-searching procedure could apply sound intensities from 10 to 115 dB SPL in 2 to 5 dB steps. *In situ* measurements of this setup (probe microphone PCB-Larson-Davis ¼ inch 2520, preamplifier PCB 480C02) connected to a frequency analyzer (Adobe Audition v.1.5)) indicated a 45 dB difference in the intensities of the main spectral peak of a 32 kHz tone burst and of its accompanying, low-frequency onset click (Fig. S8A). The acoustic spectra of 20 kHz tone bursts were similar. The difference was 45 dB regardless of the intensity of the main stimulus between 65 dB and 105 SPL, and this indicates that the growth of the artifact due to spectral splatter is linear. In masking-tuning experiments, the continuous masking tone (being continuous, it is not subject to spectral splatter) was sent through an independent electronic and acoustic channel (a second Radioshack earphone connected to the ear via a Y-shaped tube). Spectral analysis of the sound measured *in situ* indicated that there was no nonlinear interaction between masker and tone-burst.

ABR and CAP thresholds were defined as the sound level producing the smallest detectable wave, verified as reproducible within 2 dB. For CAP masking tuning curves (TCs), the probe sound was a tone-burst at a selected frequency, emitted 5 to 10 dB above the detection threshold, such that the waveform was easily visible. The frequency of the interfering continuous tone was swept over a three-octave range encompassing the probe frequency. The masking criterion from which the masking TC was built was a reduction of 50 % of the probe CAP amplitude due to the presentation of the masker tone. For growth-of-

masker studies, the probe level was increased in 5 dB steps from about 10 dB above detection threshold up to at least 20 dB louder.

Statistical significance was tested with either Student's *t* test or two-way analysis of variance coupled to the Bonferroni post-hoc test (2-way ANOVA). For all statistical tests, the limit of significance was set at  $p < 0.05$ .

#### **V- SI Appendix : References**

1. Robles L & Ruggero MA (2001) Mechanics of the mammalian cochlea. *Physiol. Rev.* 81(3):1305-1352.
2. Verpy E, *et al.* (2000) A defect in harmonin, a PDZ domain-containing protein expressed in the inner ear sensory hair cells, underlies Usher syndrome type 1C. *Nature Genet.* 26(1):51-55.
3. Boëda B, *et al.* (2002) Myosin VIIa, harmonin, and cadherin 23, three Usher I gene products, cooperate to shape the sensory hair cell bundle. *EMBO J.* 21(24):6689-6699.
4. Morales FC, Takahashi Y, Kreimann EL, & Georgescu MM (2004) Ezrin-radixin-moesin (ERM)-binding phosphoprotein 50 organizes ERM proteins at the apical membrane of polarized epithelia. *Proc. Natl Acad. Sci. USA* 101(51):17705-17710.
5. Singh AK, *et al.* (2009) Differential roles of NHERF1, NHERF2, and PDZK1 in regulating CFTR-mediated intestinal anion secretion in mice. *J. Clin. Invest.* 119(3):540-550.
6. Lefèvre G, *et al.* (2008) A core cochlear phenotype in USH1 mouse mutants implicates fibrous links of the hair bundle in its cohesion, orientation and differential growth. *Development* 135(8):1427-1437.
7. Zheng L, Zheng J, Whitlon DS, Garcia-Anoveros J, & Bartles JR (2010) Targeting of the hair cell proteins cadherin 23, harmonin, myosin XVa, espin, and prestin in an epithelial cell model. *J. Neurosci.* 30(21):7187-7201.
8. Legendre K, Safieddine S, Kussel-Andermann P, Petit C, & El-Amraoui A (2008)  $\alpha$ II/βV spectrin bridges the plasma membrane and cortical lattice in the lateral wall of auditory outer hair cells. *J. Cell Sci.* 121:3347-3356.
9. Furness DN, Katori Y, Nirmal Kumar B, & Hackney CM (2008) The dimensions and structural attachments of tip links in mammalian cochlear hair cells and the effects of exposure to different levels of extracellular calcium. *Neuroscience* 154(1):10-21.
10. Verpy E, *et al.* (2008) Stereocilin-deficient mice reveal the origin of cochlear waveform distortions. *Nature* 456(7219):255-258.
11. Le Calvez S, Avan P, Gilain L, & Romand R (1998) CD1 hearing-impaired mice. I: Distortion product otoacoustic emission levels, cochlear function and morphology. *Hear. Res.* 120(1-2):37-50.
12. Avan P, Büki B, & Petit C (2013) Auditory Distortions: Origins and Functions. *Physiol. rev.* 93(4):1563-1619.